Long-term evolution of terrestrial weathering and its link to Earth's oxygenation

Bayon Germain [1, *], Bindeman Ilya N. [2], Trinquier Anne [1], Retallack Gregory J. [2], Bekker Andrey [3, 4]

[1] Univ Brest, CNRS, Ifremer, Geo-Ocean, F-29280 Plouzané, France
[2] Department of Earth Sciences, University of Oregon, Eugene, OR 97403-1272, USA
[3] Department of Earth and Planetary Sciences, University of California, Riverside, CA 92521, USA
[4] Department of Geology, University of Johannesburg, Auckland Park 2006, South Africa

* Corresponding author : Germain Bayon, email address : gbayon@ifremer.fr

Abstract :

Terrestrial weathering releases phosphorus and other essential nutrients that fuel life in Earth's surface environments and sustain oxygenic photosynthesis. Despite previous suggestions that major changes in terrestrial chemical weathering might have played a role in the global oxygen cycle in the geological past, little is known about the Earth's weathering history. To date, the cause-and-effect relationship between weathering and the long-term evolution of atmospheric oxygen, and whether chemical weathering became more efficient after the initial rise of atmospheric oxygen in the early Paleoproterozoic, remained largely elusive. Here we report a reconstruction of the intensity of terrestrial weathering for the last 2.7 billion years, based on coupled neodymium-hafnium isotope ($\Delta \varepsilon Hf(i)CLAY$) and elemental analyses of the fine-grained clay-size fraction of shales. A pronounced shift towards higher $\Delta \varepsilon Hf(i)CLAY$ values and rubidium/aluminium (Rb/Al) ratios indicates that preferential dissolution of phosphate-bearing minerals and biotite intensified between ~2.5 and 2.4 billion years ago (Ga), following the emergence of continental landmasses and coinciding with the initiation of the Great Oxidation Event. After a long time interval characterized by a constant degree of low-intensity chemical weathering, between ~2.3 to 0.7 Ga, terrestrial weathering further accelerated after the Neoproterozoic glaciations at ~0.6 Ga, as inferred from markedly decreased Rb/Al ratios, coincident with the second rise of atmospheric oxygen. These findings support a link between the long-term intensity of chemical weathering and atmospheric oxygen level since the late Archean. We further propose that the 100-million-year-long period of enhanced terrestrial weathering from ~2.5 Ga played a major role, via crustal recycling of phosphorus and export to the surface ocean, in the early expansion of the aerobic biosphere that ultimately led to the Great Oxidation Event.

Highlights

► Geochemical investigation of the clay-size fraction of shales for the past 2.7 Ga. ► Hf-Nd isotopes and Rb/Al ratio as proxies for continental chemical weathering. ► Enhanced crustal weathering of apatite and micas between ~2.5 and 2.4 Ga. ► Marked acceleration of feldspar weathering after ~0.6 Ga. ► Co-evolution of terrestrial weathering and atmospheric oxygenation since late Archean.

1. Introduction

The oxygenation of the Earth's atmosphere has occurred in several stages over the last four billion years, driving crucial long-term changes of marine and terrestrial ecosystems (e.g., Lyons et al., 2014; Catling and Zahnle, 2020). While short-lived events of atmospheric oxygenation or 'whiffs' may have punctuated the late Archean period (Anbar et al., 2007), the initial rise of atmospheric oxygen concentration (pO$_2$) is thought to have coincided with major tectonic reorganization at the Archean-Proterozoic divide, ~2.5 billion years ago (Ga), which led to the emergence of continental landmasses, the onset of subaerial volcanism, and possibly to the so-called Great Oxidation Event (GOE) between ~2.45 and 2.1 Ga (Kump and Barley, 2007). A second major step in oxygenation took place more than one billion years later during the late Proterozoic Eon (e.g., Lyons et al., 2014), following a series of major 'Snowball Earth' glaciations. Finally, near-to-modern pO$_2$ levels were established during the Devonian Period, about 400 million years ago (Ma), during the mid-Paleozoic Oxygenation Event (Dahl et al., 2010; Lenton et al., 2016). In recent years, many studies have suggested a link between the rise of oxygen in the Earth's atmosphere and continental chemical weathering (e.g., Kennedy et al., 2006; Planavsky et al., 2010; Konhauser et al., 2011; Lenton et al., 2012; Bekker and Holland, 2012; Reinhard et al., 2017), in particular for its importance in delivering nutrients essential to life and oxygenic photosynthesis to the aqueous environments. Upon weathering, substantial amounts of the ultimate limiting nutrient, phosphorus (P), are exported to terrestrial and marine environments, where they sustain primary productivity and subsequent organic carbon burial in the sedimentary record (Planasky et al., 2010). Because this process represents the major long-term source of oxygen to the atmosphere, rising atmospheric oxygen level during the late Neoproterozoic has been linked to accelerated continental weathering and increased P flux in the aftermath of 'Snowball Earth' glaciations (Planavsky et al., 2010; Reinhard et al., 2017). Similarly, the Devonian rise of land plants and its impact on the export of P to surface

environments, via enhanced chemical weathering, might have caused the mid-Paleozoic Oxygenation Event (Lenton et al., 2016). Additionally, multiple evidence for accumulation of redox-sensitive metals and/or changes in their isotopic compositions (e.g., molybdenum, rhenium, chromium, arsenic, uranium and thallium) in late Archean sedimentary records have also been interpreted as reflecting the onset of mild oxidative weathering of crustal sulphide minerals at ~2.5 Ga (e.g., Anbar et al., 2007; Konhauser et al., 2011; Ostrander et al., 2021, and references therein). While sulphide weathering itself acts a net sink for atmospheric O_2, the above-mentioned metal enrichments and isotopic shifts were taken as possible indirect indicators of the enhanced export of land-derived P and other bio-essential elements to surface ocean (e.g., Konhauser et al., 2011), which could have promoted primary productivity and, in turn, paved the way for the GOE. Nevertheless, despite its potential importance in driving the rise of atmospheric oxygen over Earth's history, the long-term evolution of terrestrial weathering remains largely undefined.

Here, we present a novel approach, based on the application of elemental geochemistry and combined lutetium-hafnium / samarium-neodymium isotope systematics to fine-grained siliciclastic sedimentary rocks worldwide (Fig. 1), which provides new insight into feedbacks linking chemical weathering, continental inputs of nutrients to the oceans, and atmospheric oxygen level since the late Archean.

2. Reconstructing past weathering using proxies applied to clay-size detrital fraction

Over the past decades, a variety of proxies has been employed for reconstructing the evolution of weathering in deep time, based on carbonate record of ancient seawater chemistry (e.g., Shields and Veizer, 2002), and on the mineralogical and geochemical composition of paleosols and other fine-grained siliciclastic rocks (e.g., Cox et al., 1995; Kennedy et al., 2006). While providing important insight to past continental weathering and associated fluxes to the ocean,

the inferences that can be drawn from the use of bulk-rock or carbonate geochemistry are limited, due to possible source effects and various other processes, such as post-depositional remobilization, mineral sorting and grain-size control, which can affect proxy record (e.g., Fedo et al., 1995; Shields and Veizer, 2002). In particular, ancient fine-grained sedimentary rocks such as shales are prone to various depositional, diagenetic, and metamorphic processes, which can obscure the chemical weathering signal. Shales are indurated mixtures of clays generated via continental weathering and unweathered detrital minerals such as quartz, feldspar, and heavy accessory minerals (e.g., zircons), together with authigenic minerals and organic compounds. Whenever possible, analysing the separated clay-size fraction of siliciclastic sediments is generally best suited to access chemical weathering and environmental conditions at the time of clay production in soils (e.g., Bayon et al., 2016; Bayon et al., 2021).

Among the set of demonstrated proxies for modern continental weathering, the combined use of neodymium (Nd) and hafnium (Hf) isotope ratios in detrital clays offers a great potential for applications to deep-time sedimentary records. Terrestrial rocks define a broad correlation trend for Nd and Hf isotope ratios, termed the Terrestrial Array (Fig. 2a; Vervoort et al., 1999), which results from the covariant behaviour of samarium-neodymium and lutetium-hafnium parent-daughter isotope pairs during magmatic processes. At the mineral scale, however, Lu and Hf are partitioned differently into rock-forming minerals, much more strongly than Sm and Nd, leading with time and radioactive decay to mineral phases having markedly different Hf isotopic compositions. In most rocks, Hf budget is dominated by weathering-resistant zircons having low Lu/Hf ratios and thus relatively unradiogenic (low) ε_{Hf} signature compared with other rock-forming minerals. Because zircons are preferentially enriched in coarse-grained detrital fractions during sediment transport and depositional processes (Patchett et al., 1984; Garçon et al., 2013; Bayon et al., 2016), the finest clay-size fraction displays comparatively

more radiogenic Hf isotope composition (e.g., Bayon et al., 2016), defining a distinctive correlation in the ε_{Nd} vs. ε_{Hf} plot, referred to as the Clay Array (Bayon et al., 2016; Fig. 2a). Additionally, continental chemical weathering leads to preferential dissolution of Lu-rich mineral phases, thereby commonly releasing highly radiogenic Hf to the surface environments (Bayon et al., 2006; Dausmann et al., 2019). Because secondary clay minerals form in soils, they incorporate a fraction of radiogenic Hf previously released via rock alteration (Bayon et al., 2016). As a consequence, the 'vertical' deviation of any clay-size sediment relative to the Clay Array in the ε_{Nd} vs. ε_{Hf} plot (hereafter referred to as $\Delta\varepsilon_{Hf\,CLAY}$) reflects the relative proportion of secondary clays (with high ε_{Hf} values) to primary (unweathered) minerals (with lower ε_{Hf} values) (Bayon et al., 2016). In modern river systems, $\Delta\varepsilon_{Hf\,CLAY}$ directly relates to chemical weathering intensity and its controlling parameters, as illustrated by direct relationship with mean annual temperature (MAT) in corresponding drainage basins (Fig. 3). Because REE and Hf are highly immobile elements, both Lu-Hf and Sm-Nd isotopic systems in fine-grained siliciclastic sediments are unlikely to be significantly disturbed by post-depositional processes such as diagenesis, reverse weathering (see discussion below), and low-grade metamorphism (Ohr et al., 1994; Hoffmann et al., 2010), this measure of Hf-Nd isotope decoupling ($\Delta\varepsilon_{Hf\,CLAY}$) can hence be used for ancient sedimentary records as a robust proxy for chemical weathering. Importantly, in contrast to conventional weathering indices based on elemental ratios, $\Delta\varepsilon_{Hf\,CLAY}$ can constrain dissolution of highly radiogenic phosphate-bearing minerals such as apatite during continental chemical weathering. Because apatite represents the main source of the bio-essential nutrient P on Earth (e.g., Planavsky et al., 2010; Reinhard et al., 2017), this makes $\Delta\varepsilon_{Hf\,CLAY}$ a unique proxy for identifying past weathering events associated with release of biologically limiting P, and thus, for investigating the potential links between continental chemical weathering and atmospheric oxygenation.

In this study, we also use the rubidium/aluminium ratio (based on the degree of feldspar weathering and higher mobility of Rb compared to Al during chemical weathering) as a complementary proxy for silicate rock weathering, which also demonstrates a clear relationship with climate and chemical weathering intensity in modern detrital clays (Fig. 3). In endogenic processes, Rb is closely linked with potassium (K), being enriched in resistant K-bearing minerals such as feldspar. Significant amounts of Rb also occur in biotite and other mica minerals that are preferentially dissolved during the early stages of weathering (Nesbitt and Markovics, 1980; Erel et al., 2004). During chemical weathering, Rb is preferentially retained in soils relative to K (e.g., Nesbitt and Markovics, 1980), which results in secondary clays generally displaying higher Rb abundances than coarser-grained detrital fractions (Bayon et al., 2021). Compared with K and other major mobile elements (e.g., Na and Mg), Rb is also generally depleted in seawater and in other fluids that can contribute, through various water-rock interactions, to post-depositional rock alteration such as metasomatism (e.g., van de Kamp, 2016). Consequently, this implies that the Rb/Al ratio in ancient, fine-grained, sedimentary rocks is less likely to be affected by post-depositional water-rock interaction, compared to other weathering proxies, based on more mobile elements, such as K/Al ratio or the chemical index of alteration (CIA). In this study, another potential complication with the use of weathering proxies in clay-size fraction of ancient shales could possibly arise from the recycling of older material formed during previous sedimentary cycles (e.g., Gaillardet et al., 1999). Nevertheless, past studies indicate that the clay-size material eroded from ancient sediments still provides useful information on present-day weathering conditions (e.g., Dere et al., 2013). Thus sedimentary recycling is unlikely to affect significantly the interpretation of our weathering proxy records.

3. Samples and Methods

A suite of shales and other fine-grained sedimentary rocks (n=107) of different ages was analysed for neodymium and hafnium isotope ratios, together with major and trace element abundances (see Supplementary Material, Section S1; Table S1; Fig. 1). Shales can provide a unique integrated record for the chemical evolution of the eroded and weathered upper continental crust through time (e.g., Greber et al., 2017; Garçon, 2021). The degree of metamorphism of the studied shale units is not higher than the lower greenschist facies. Additionally, previous studies of the same suite of samples as analysed here have already demonstrated its utility for reconstructing past environmental conditions on continents (e.g., Greber et al., 2017; Bindeman et al., 2018). All studied samples were first cleared of biogenic, authigenic, and organic components, and subsequently centrifuged in order to separate the finest clay-size (<2 µm) fraction from the residual coarse-grained and zircon-bearing detritus (see Supp. Mat. S2). All clay-size fractions of samples for which the presence of zircon was suspected were excluded from the discussion below (see Supp. Mat. S3; Fig. S1).

4. Results

Data for major and trace elements, and Hf-Nd isotopic compositions are listed in Table S2 and Table S3, respectively. As expected, most clay-size fractions considered in this study fall within the fields of Hf-Nd isotopic composition defined by the present-day Terrestrial and Clay arrays (Fig. 2a). After correction for radioactive decay (see Supp. Mat. S2), most initial ε_{Nd} and ε_{Hf} values of clay-size fraction from the late Archean and some Proterozoic samples plot on (or near) the initial Terrestrial Array (Fig. 2a). All other studied samples, including many from the late Archean to early Paleoproterozoic, ~2.5-2.4 Ga ago, display comparatively more radiogenic Hf isotopic compositions and lie closer to the Clay Array, hence suggesting that

Earth's continental chemical weathering and accompanying Hf-Nd isotope decoupling operated since at least the late Archean to early Proterozoic (Fig. 2a).

Further, most studied clay-size fractions plot within the field defined by modern detrital clays for K/Rb, K/Al, and K/Rb ratios (Fig. 4). A few samples, mostly from the late Archean, ~2.73-2.50 Ga, time interval display higher K/Rb values (>240), which significantly depart from measured ratios in modern clays (153 ± 40, 1 SD; Table S2). Because such values could possibly reflect the influence of post-depositional hydrothermal processes, these samples were excluded below when discussing the long-term evolution of Rb/Al (and K/Al) in the shale record. Note also that samples from the late Archean to early Paleoproterozoic, 2.50-2.39 Ga, are characterized by much higher Rb/Al ratios (up to ~0.0037; Fig. 4). While plotting outside the field defined by modern clays, theoretical curves reflecting hydrothermal contribution to detrital clays suggest that such Rb/Al values are unlikely to be generated by K-metasomatism (Fig. 4), pointing instead, as will be proposed below, towards a putative effect of biotite dissolution.

5. Discussion

5.1. Potential effect of reverse weathering and marine clay authigenesis

Recently, a number of studies have suggested that extensive authigenic clay mineral formation occurred in Precambrian oceans due to much higher dissolved silica concentration in seawater (Isson and Planavsky, 2018). In modern marine sediments, *in situ* formation of authigenic clays is driven by dissolution of reactive phases such as biogenic silica, Fe-Mn oxyhydroxides and/or primary phyllosilicate minerals (Michalopoulos and Aller, 1995). This process is referred to as reverse weathering, because unlike continental weathering of silicate rocks, it acts as a net source of CO_2 to the atmosphere-ocean system. Until the emergence of silica biomineralizers

at the start of the Phanerozoic Eon, reverse weathering presumably played an important role in the global carbon cycle and climate, possibly explaining the formation of Fe-rich clay minerals preserved in the ancient sedimentary record (Isson and Planavsky, 2018). While the behaviour of REE and Hf during reverse weathering remains poorly documented, the REE cycling associated with marine clay authigenesis seems to be closely linked to dissolution of detrital clay minerals (Abbott et al., 2019). Additionally, previous studies have shown that an increased degree of authigenic clay precipitation in marine sediments (i.e. reflecting higher contribution of seawater and/or pore water) is accompanied by a net loss of REE in neoformed clay minerals compared to the average REE content in detrital clays (e.g., Stille and Clauer, 1994). Based on the above, we infer that clay mineral authigenesis in Precambrian oceans did not have a major impact on the distribution of REE and Hf in the fine-grained siliciclastic sediments deposited at the seafloor and subsequently preserved in the shale record. Therefore, in the discussion below, the influence of reverse weathering and marine clay authigenesis on our weathering proxy data is considered negligible.

5.2. Decoupling of terrestrial weathering from the long-term evolution of the continental crust since the late Archean

Prior to using Rb/Al and $\Delta\varepsilon_{Hf(i)CLAY}$ in studied clay-size fraction as proxies of past terrestrial weathering care must also be taken to assess whether observed variations could reflect compositional change in the upper continental crust through time. While the chemical evolution of the continental crust over Earth history is still subject to debate, there is consensus that it has remained mostly unchanged since the early Proterozoic (e.g., Condie, 1993; Greber et al., 2017). In this study, this is illustrated by the fact that the Ni/Co ratio, i.e. a provenance tracer for ultramafic versus mafic-felsic crustal material contribution (e.g., Condie, 1993), displays near-constant values over the past 2.5 Ga (4 ± 3, 1 SD; n=73; Fig. 5a; Table S2), similar to

those for modern detrital clays (4 ± 1; Table S4). In contrast, late Archean shales exhibit much

higher Ni/Co values (14 ± 8; n=28; Table S4), indicating, as previously suggested (e.g., Condie,

1993; Greber et al., 2017), larger contribution of detrital sediments derived from the erosion of

ultramafic (komatiitic) rocks prior to 2.5 Ga. Changes in the nature of the exposed continental

crust can also be inferred using Nd-depleted mantle model ages (T_{DM}), which provide an

estimate for the mean age of mantle extraction in the provenance (see Supp. Mat. S4). In the

shale record, the difference between T_{DM} and corresponding depositional age (T_{DEP}) indicates

the average age of eroded source rocks (or mean crustal residence time; Fig. 5b), and represents

a qualitative measure of the presence of juvenile versus mature crustal material in the

provenance. When considering studied samples and other fine-grained sedimentary rocks (Fig.

5b), the age estimates of eroded crustal materials display a long-term trend towards a more

mature continental crust through time (i.e. older provenance), reflecting a gradual aging of the

upper continental crust since the late Archean (e.g., Allègre and Rousseau, 1984). A second-

order variability in mean crustal residence age also indicates a possible link with the periods of

assembly and breakup of supercratons/supercontinents over the past 3 Ga (see vertical grey bars

in Fig. 5), which are associated with increased production rate of juvenile continental crust and

relative tectonic quiescence, respectively (e.g., Condie, 2004). Importantly, in this study,

neither Rb/Al nor $\Delta\epsilon_{Hf\ CLAY}$ appear to follow the long-term chemical evolution and/or nature of

the continental crust inferred from Ni/Co and T_{DM}. For Rb/Al (Fig. 5d), two major changes

occurred over the last 2.7 Ga: a shift towards higher values between ~2.50-2.39 Ga (with mean

Rb/Al ~ 0.0025 ± 0.0005; 1SD; n=18; Table S2) and fall to lower values after ~0.6 Ga (with

mean Rb/Al 0.0012 ± 0.0004; 1SD; n=34). In contrast, for the most of the Proterozoic, between

~2.32 and 0.70 Ga, clay-size fraction displays near-constant Rb/Al ratio (0.0016 ± 0.0003;

n=22; Fig. 5d). The long-term evolution of $\Delta\epsilon_{Hf\ CLAY}$ values in our shale record also documents

a pronounced shift from the late Archean (~2.73-2.60 Ga) period (with mean $\Delta\epsilon_{Hf\ CLAY}$ ~ -3.3

± 2.3, 1 SD; n=9; Table S3) towards more radiogenic values between ~2.5-2.39 Ga, with a mean $\Delta\varepsilon_{Hf\ CLAY} \sim +0.9 \pm 3.5$ (n=19; Fig. 5e). During the subsequent Proterozoic and Phanerozoic eons, no obvious secular trend can be observed (Fig. 5e), with indices of Nd-Hf isotope decoupling encompassing the large range of $\Delta\varepsilon_{Hf\ CLAY}$ values observed in modern terrestrial environments (Fig. 2). Overall, the absence of any apparent correlation between our Rb/Al and $\Delta\varepsilon_{Hf\ CLAY}$ indices and the long-term chemical evolution of the continental crust since the late Archean to early Paleoproterozoic provides reassurance about their reliability as weathering proxies, at least over the past ~2.5 Ga.

5.3. A pulse of continental crust weathering between 2.5 and 2.4 Ga

A striking feature of our results is the sharp shift towards positive $\Delta\varepsilon_{Hf(i)CLAY}$ values and higher Rb/Al ratios between ~2.5 and 2.4 Ga (Fig. 6), which, based on the above consideration, can be best interpreted as reflecting a major change in terrestrial weathering. The late Archean to early Paleoproterozoic coincides with a profound reorganization of Earth's surface environments, which resulted from the emergence of large continental landmasses, subsequent emplacement of series of Large Igneous Provinces (LIPs) onto these landmasses, and onset of the modern hydrological cycle (e.g., Kump and Barley, 2007; Bindeman et al., 2018; Ernst et al., 2021). As discussed above, this major tectonic transition in Earth history is recorded in studied clay-size fraction by the abrupt fall of the Ni/Co ratio after ~2.5 Ga (Fig. 6b), which marks the decrease in sediment flux derived from komatiitic rocks (with high Ni/Co ratio) and increasing input of material associated with the erosion of mafic and felsic rocks (with low Ni/Co ratios). In this context, our proxy data suggests that subaerial weathering of the newly emerged upper continental crust at that time was accompanied by the formation of clay minerals having both radiogenic Hf isotope composition and high Rb/Al ratios. This chemical weathering pattern is in stark contrast to what is observed in modern terrestrial environments, where radiogenic

positive $\Delta\epsilon_{Hf(i)CLAY}$ values generally coincide, under intense chemical weathering conditions, with low Rb/Al ratios in detrital clays (Fig. 3). Alternatively, positive $\Delta\epsilon_{Hf(i)CLAY}$ values are also encountered in modern sediments derived from extensive areas with volcanic rocks (Table S4). To date, high $\Delta\epsilon_{Hf(i)CLAY}$ values (up to +3.5; Table S4) have been reported in volcanogenic sediments from the British Tertiary volcanic province and also from younger volcanically active regions (e.g., North Island of New Zealand; Kamchatka Peninsula of Russia). These modern examples indicate that basalt weathering also results in the preferential dissolution of weathering-susceptible Lu-rich minerals such as apatite, eventually leading to the formation of detrital clays having radiogenic Hf compositions, even in young volcanic provinces and under cold climatic conditions (Bayon et al., 2016). By analogy, the highly positive $\Delta\epsilon_{Hf(i)CLAY}$ values observed in the shale record after ~2.5 Ga could hence reflect the early weathering stage of subaerial, juvenile, mafic volcanic rocks associated with preferential dissolution of apatite and other Lu-rich minerals. This interpretation is in line with our T_{DM} model ages, which indicate the overwhelming presence of juvenile crustal material (i.e. with young T_{DM} ages) in corresponding samples, but also with evidence for widespread subaerial volcanism at the late Archean to early Paleoproterozoic and emplacement of LIPs (Kump and Barley, 2007; Ernst et al., 2021).

Concerning Rb/Al, as discussed above, the high ratios in the clay-size fraction of ~2.5 to 2.4 Ga shales is unlikely to be related to K-metasomatism. Nevertheless, several studies have suggested that the ~2.5 Ga shales of the Mount McRae Formation from the Pilbara craton (Western Australia) could have been hydrothermally altered at ~2.2 Ga (e.g., Rasmussen et al., 2005; Slotznick et al., 2022). Because hydrothermal fluids can be occasionally associated with high Rb content and low K/Rb ratios < 200 (e.g., van de Kamp, 2016), metasomatic alteration could potentially account for the observed high Rb/Al ratios (Fig. 4). However, this hypothesis

seems unlikely for two reasons. First, samples from the ~2.44 Ga Turee Creek Group, i.e. a slightly younger sedimentary succession from the same Pilbara craton, display extremely low Rb/Al (≤0.0003) and high K/Rb (780 to 1240; Fig. 4) values, which, despite showing clear sign of hydrothermal overprint, suggests that the ~2.2 Ga regional, hydrothermal event cannot explain the high Rb/Al ratios in the Mount McRae Shale. Second, other early Paleoproterozoic mudstones from the Pecors and McKim formations of the lower Huronian Supergroup (Ontario, Canada) also display high Rb/Al ratios (> 0.0018; Table S2), although showing no evidence of any metasomatic alteration (McLennan et al., 2000). Therefore, we are confident that the high Rb/Al ratios in the clay-size fraction from mudstones deposited during the late Archean to early Paleoproterozoic cannot be attributed to metasomatic processes.

Instead, we propose that such high Rb/Al ratios are best explained by preferential alteration of biotite and other Rb-rich mica minerals. Atmospheric partial pressure of oxygen (pO$_2$) across the Archean–Proterozoic boundary was very low, with pO$_2 < 10^{-5}$ present atmospheric level (Pavlov and Kasting, 2002). Nevertheless, experimental work showed that biotite could effectively weather under the low oxygen level of the late Archean atmosphere, leading to formation of secondary clays such as vermiculite and smectite at the edge of biotite grains (Murakami et al., 2004). Experimental studies also indicate that the very early stages of chemical weathering are typically associated with dissolution of accessory minerals (e.g., apatite, sphene, and trace calcite) and leaching from the interlayer sites of biotite and other micas (e.g., Erel et al., 2004). Therefore, on this basis, we infer that between ~2.5 and 2.4 Ga, exposure of fresh, juvenile, volcanic rocks associated with LIPs, prone to chemical alteration, resulted in the preferential release of radiogenic Hf (due to dissolution of apatite and other Lu-rich minerals) and Rb (due to incongruent weathering of biotite and other mica minerals), which were subsequently incorporated into secondary clay minerals.

5.4. Evidence for reduced continental weathering during the Proterozoic

Between ~2.4 and 2.2 Ga, Earth experienced four global glaciations (Bekker and Holland, 2012; Fig. 6). At that time, a combination of continental emergence and recurring glacial conditions led to an acceleration of erosional processes. During this glacially influenced period, the predominance of physical erosion led to deposition of fine-grained sedimentary rocks dominated by primary detrital mineral assemblages, thereby explaining the observed shift towards negative $\Delta\varepsilon_{Hf(i)CLAY}$ values (Fig. 6). A similar effect has been observed in modern environments, where fluvial clays from cold regions systematically exhibit negative $\Delta\varepsilon_{Hf(i)CLAY}$ values (Bayon et al., 2016; Fig. 3). This interpretation is also consistent with the measured Rb/Al ratios, which display, after 2.4 Ga, values similar to those encountered in modern catchments characterized by low intensity of chemical weathering and dominated by physical erosion processes (0.0018 ± 0.0003; Fig. 3). In fact, the striking constancy of Rb/Al ratios observed between ~2.3 and 0.7 Ga (Fig. 5), with an almost identical mean value of 0.0016 ± 0.0003 (1 SD), indicates that reduced chemical weathering conditions most likely prevailed during almost the entire Proterozoic Eon. This finding is consistent with recent work pointing at limited pedogenic clay mineral formation during this period (Rafiei and Kennedy, 2019; Rafiei et al., 2020; Retallack et al. 2021). A low degree of silicate weathering during the Proterozoic is also supported by K/Al ratios, which display a range (0.32 ± 0.06, 1 SD; n=22; Table S2) between ~2.32 and 0.70 Ga similar to that observed in river clays in cold climate settings (0.32 ± 0.06; Fig. 3).

In contrast, our clay-size fractions exhibit a much larger variability for coupled Nd-Hf isotope systems across the Proterozoic, with many shales even displaying positive $\Delta\varepsilon_{Hf(i)CLAY}$ values up to +6.3 (Fig. 5; Table S3). Considering the above-mentioned evidence for reduced continental

weathering during the Proterozoic, such radiogenic Hf signatures are best explained as reflecting the incongruent weathering of volcanic rocks associated with preferential alteration of Lu-rich minerals, followed by subsequent Lu incorporation into secondary clays. This is consistent with the radiogenic Nd signature of corresponding samples (having $\varepsilon_{Nd(i)}$ between ~ -3 and 0; Table S3) and their relatively short mean crustal residence time (<1000 Ma), indicating that these high $\Delta\varepsilon_{Hf(i)CLAY}$ values are indeed related to the presence of juvenile mafic rocks in their provenance.

To summarize, despite the evidence indicating that physical weathering was prevalent in vegetation-free Precambrian terrestrial environments, resulting in the export of fine-grained sediments dominated by detrital mineral assemblages, our results suggest that pervasive dissolution of accessory Lu-rich mineral phases, such as apatite, remained important during the Proterozoic in association with preferential weathering of juvenile mafic crustal rocks.

5.5. Accelerated feldspar weathering started with the late Neoproterozoic

For Hf-Nd isotopes, the relatively low temporal resolution in this study and the fact that studied samples come from diverse geographical locations (Fig. 1), and were presumably formed under different climatic conditions, probably both account for the absence of any secular trend of $\Delta\varepsilon_{Hf(i)CLAY}$ from the late Neoproterozoic onwards (Fig. 7b). During the Phanerozoic, short-term (~10-Myr) variations in intensity of chemical weathering were likely driven by changes in global climate and atmospheric carbon dioxide level, and their feedbacks with tectonics and orogenesis (e.g., Raymo and Ruddiman, 1992; MacDonald et al., 2019). For instance, a recent study of combined Hf-Nd isotope ratios of clay-size fraction of marine sediments suggested that global cooling during the Late Cretaceous was linked to intense silicate weathering and associated drawdown of atmospheric carbon dioxide, following tectonic uplift of the southern

part of South American continent (Corentin et al., 2022). When exposed at the Earth's surface, highly weatherable rocks, such as basalts or any other mafic or ultramafic rocks, are subject to intense erosion and their dissolution acts as a major sink for atmospheric CO_2 (e.g., Dessert et al. 2003). This process is particularly intense when tectonic uplift occurs in low-latitude regions, where warm and wet conditions can result in significant erosion-driven CO_2 consumption, ultimately leading to global cooling (e.g., MacDonald et al., 2019). In this study, temporal resolution is however insufficient to assess possible relationship between continental weathering and global climate change during the Phanerozoic, as illustrated in Fig. 7 by the lack of apparent correlation between our weathering proxy records and the timing of major glaciations.

Nevertheless, a long-term gradual fall in Rb/Al and K/Al ratios of clay-size fraction of studied shales can be observed after ~0.6 Ga (Fig. 7), consistent with an earlier observed weathering trend based on fine-grained sedimentary rocks from the Russian and North American platforms (e.g., Cox et al., 1995). In agreement with the inferred enhanced clay production at the end of the Proterozoic (Kennedy et al., 2006), our proxy data provide direct indication that chemical weathering of resistant K-feldspar intensified on continents after the Neoproterozoic glaciations (Fig. 7). The subsequent rise of vascular plants further enhanced terrestrial weathering after ~400 Ma, due to the combined impact of roots and associated fungi in soils (e.g., Lenton et al., 2016). In turn, accelerated K-feldspar weathering in soils at that time also presumably paved the path for the appearance of higher plants during the Devonian Period, due to their high potassium requirements (Basu, 1981), consistent with the observed trends in our shale record towards lower Rb/Al and K/Al ratios after ~400 Ma (Fig. 7).

5.6. Co-evolution of continental weathering and atmospheric oxygenation since the late Archean

The long-term variations in intensity of terrestrial weathering inferred from our proxy data provide support for a link with the evolution of atmospheric oxygen over the past 2.7 Ga. The late Archean to early Paleoproterozoic enhanced weathering event inferred from Hf isotopes and Rb/Al ratios between ~2.5 and 2.4 Ga coincides with a well-documented episode of mild environmental oxygenation pre-dating the GOE (e.g., Anbar et al., 2007; Konhauser et al., 2011; Ostrander et al., 2021) and emplacement of series of LIPs globally (Ernst et al., 2021). Collectively, these studies reporting enrichments and isotopic shifts for redox-sensitive elements in ~2.5 Ga marine shales have amassed evidence for oxidative weathering of crustal sulphides at the end of the Archean Eon. Our new proxy data show that this transient episode of early atmospheric oxygenation was also associated with preferential dissolution of other weathering-susceptible, non-sulphide mineral phases, such as mica minerals and apatite. Experimental study has demonstrated that incongruent dissolution of biotite is possible under low pO$_2$ levels of the Archean (Murakami et al., 2004). While the direct influence of pO$_2$ on phosphate-bearing mineral dissolution is uncertain (Goyne et al., 2006), apatite weathering between ~2.5 and 2.4 Ga would have been greatly enhanced by aerobic microbial activity and low pH in soils (Guidry and Mackenzie, 2000; Neaman et al., 2005; Goyne et al., 2006). The development of such conditions in the late Archean to early Paleoproterozoic is supported by proxy evidence for accelerated dissolution of terrestrial sulphides at that time, which was attributed to aerobic bacterial oxidation and is thought to have resulted in acidic groundwaters and sulfuric-acid-driven weathering of the exposed upper continental crust (Konhauser et al., 2011; Bekker and Holland, 2012).

For the most of the Proterozoic, reduced continental chemical weathering most likely prevailed under low level of atmospheric O_2, as inferred from the relatively high Rb/Al ratios observed in clay-size fraction of ~2.3 to 0.7 Ga shales. From ~0.6 Ga, our weathering proxy data again indicate the strong causal relationship between Earth's surface oxygenation and intensity of terrestrial weathering in the aftermath of the Neoproterozoic glaciations and subsequent rise of atmospheric oxygen (Fig. 7). The stepwise increase in pO$_2$ from low concentrations of the mid-Proterozoic was accompanied by corresponding shift towards lower Rb/Al and K/Al ratios indicative of accelerated weathering of resistant K-feldspar (Fig. 7). The early Paleozoic shift towards enhanced global weatherability of continental rocks is further supported by a marked change in the strontium isotopic composition of seawater, which indicates substantially increased dissolved continental flux to the ocean at that time (e.g., Shields and Veizer, 2002; Kennedy et al., 2006), coincident with the Pan-African orogeny (Merdith et al., 2021). While the intensity of K-feldspar weathering during the Devonian was partly driven by the advent of vascular plants on land, we hypothesize that the pO$_2$ rise at the end of the Neoproterozoic could have also resulted in enhanced weathering of redox-sensitive, Fe-bearing, silicate minerals, such as pyroxenes and olivine. Oxidative dissolution experiments with ferromagnesian minerals indicate the development of surficial coating of hydrated Fe-oxides, which can severely reduce mineral dissolution rates under oxygenated conditions (Schott and Berner, 1985). However, highly productive soil microbiomes and later evolution of higher plants and trees during the Phanerozoic greatly increased soil organic ligand content and acidity (Basu, 1981; Lenton et al., 2012; Lenton et al., 2016), which most likely inhibited formation of such protective Fe-oxide coatings and resulted in enhanced biological and chemical silicate weathering (Schott and Berner, 1985).

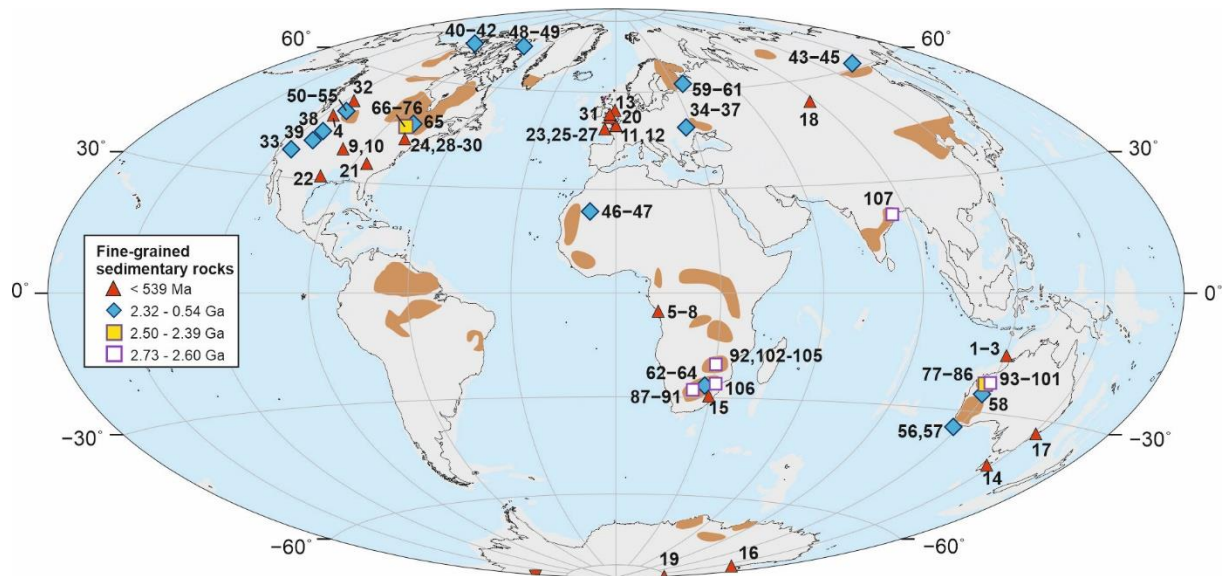## 6. Concluding remarks and implications

Overall, our geochemical investigation of the clay-size fraction of shales suggests that the long-term increase in terrestrial chemical weathering was coupled with atmospheric O_2 levels over Earth's history. The empirical relationship between atmospheric oxygen level and weathering intensity proxy data further suggests that the response of chemical weathering to changes in pO_2 was controlled by the stability of rock-forming minerals, resulting in incongruent, likely microbially mediated, dissolution processes that preferentially released phosphorus, potassium, and other bio-essential elements to the surrounding environment. Importantly, our data provide the first direct evidence for the onset of terrestrial weathering during the late Archean to early Paleoproterozoic, following emergence of large continental landmasses. Between ~2.5 and 2.4 Ga, our weathering proxy record suggests that sustained dissolved continental fluxes of apatite-derived phosphorus and other essential nutrients to surface environments and oceans promoted marine primary production and oxygenic photosynthesis, eventually counter-balancing oxygen sinks and ultimately leading to the GOE. This further supports that terrestrial chemical weathering may have been instrumental in driving the long-term evolution of biosphere on Earth (cf. Konhauser et al., 2011; Bekker and Holland, 2012; Guidry and Mackenzie, 2000), with higher atmospheric oxygen levels resulting in more intense terrestrial chemical weathering and enhanced flux of nutrients to the oceans.

Contributions

G.B. and I.N.B. conceived the study. A.B., I.N.B., and G.R. selected and provided the samples. G.B. performed all sample and chemical preparations, and measured their Nd-Hf isotopic compositions with A.T. All the authors contributed to data interpretation and writing the manuscript.

Acknowledgments

Figure 1. Location of studied samples showing the Archean cratons (modified from Bleeker, 2003). See Table S1 in the Supplementary Material for coordinates of all locations.
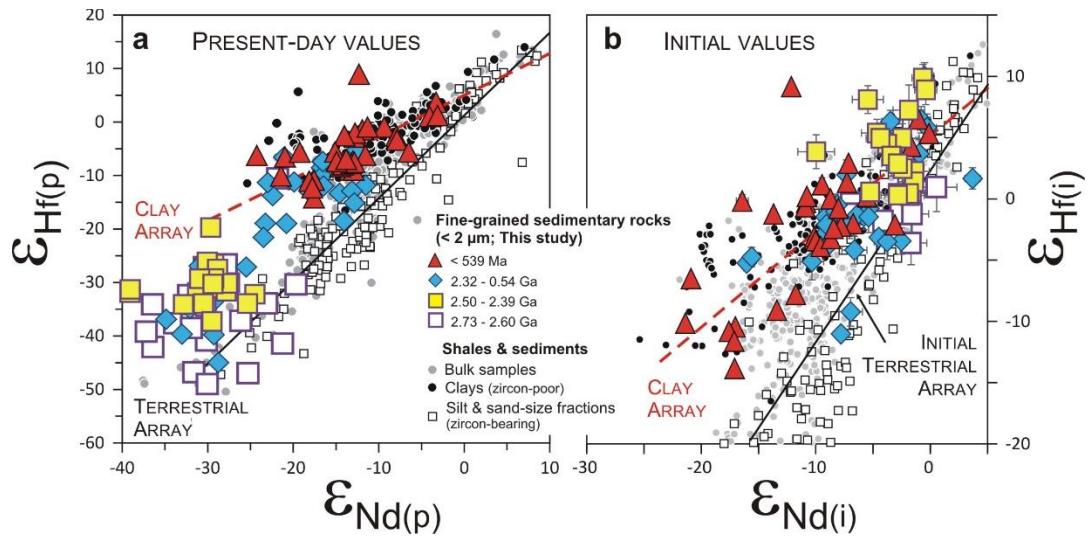
Figure 2. Neodymium and hafnium isotopic composition of clay-size fraction of fine-grained sedimentary rocks and modern sediments. **a,** Present-day ε_{Nd} and ε_{Hf} values. The Terrestrial Array ($\varepsilon_{Hf} = 1.55 \times \varepsilon_{Nd} + 1.21$; Vervoort et al., 2011) corresponds to the trend defined by all terrestrial rocks, including bulk sedimentary rocks, while the Clay Array ($\varepsilon_{Hf} = 0.78 \times \varepsilon_{Nd} + 5.23$) refers to the linear regression based on fluvial clays and clay-size fraction of modern sediments (Bayon et al., 2016). **b,** Initial ε_{Nd} and ε_{Hf} values for fine-grained sedimentary rocks are shown together with the Clay Array and the initial Terrestrial Array (black line; $\varepsilon_{Hf} = 1.39 \times \varepsilon_{Nd} + 2.29$; Vervoort et al., 2011). The deviation of fine-grained sedimentary rocks from the Terrestrial Array reflects the combination of mineralogical sorting (e.g., separation of zircons having low ε_{Hf} composition) and preferential alteration of apatite and other Lu-rich minerals by chemical weathering (resulting in the formation of secondary clays having high ε_{Hf} composition). Data for bulk shales and sedimentary rocks, and clay- and silt-size sediment fractions are from Vervoort et al. (2011) and Bayon et al. (2016), and references therein.
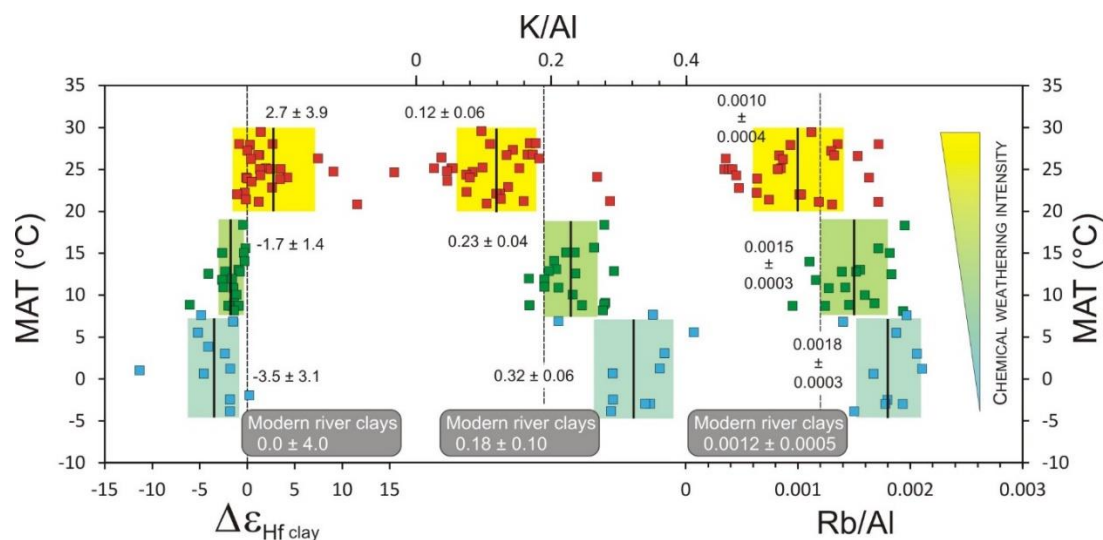
Figure 3. Relationship among weathering proxies of clay-size fraction of modern fluvial sediments and mean annual temperature (MAT) of corresponding basins. $\Delta\varepsilon_{Hf\,CLAY}$ (i.e., the ε_{Hf} deviation of fine-grained sediments from the Clay Array) reflects the relative proportion of secondary clays with radiogenic (high) ε_{Hf} composition to primary unweathered minerals with unradiogenic (low) ε_{Hf}, and the preferential alteration of Lu-rich mineral phases such as apatite. The potassium/aluminium (K/Al) ratio indicates the degree of K-feldspar alteration. The range of rubidium/aluminium (Rb/Al) ratios in river clays is controlled by biotite vs. K-feldspar chemical weathering in corresponding catchments. Mean average ± 1 SD values for studied weathering proxies are given for all catchments (dashed black lines) and for catchments in cold (MAT <8°C), temperate (8°C < MAT <20°C), and warm (>20°C) climate settings, respectively (black lines). All data and references are listed in Table S4.
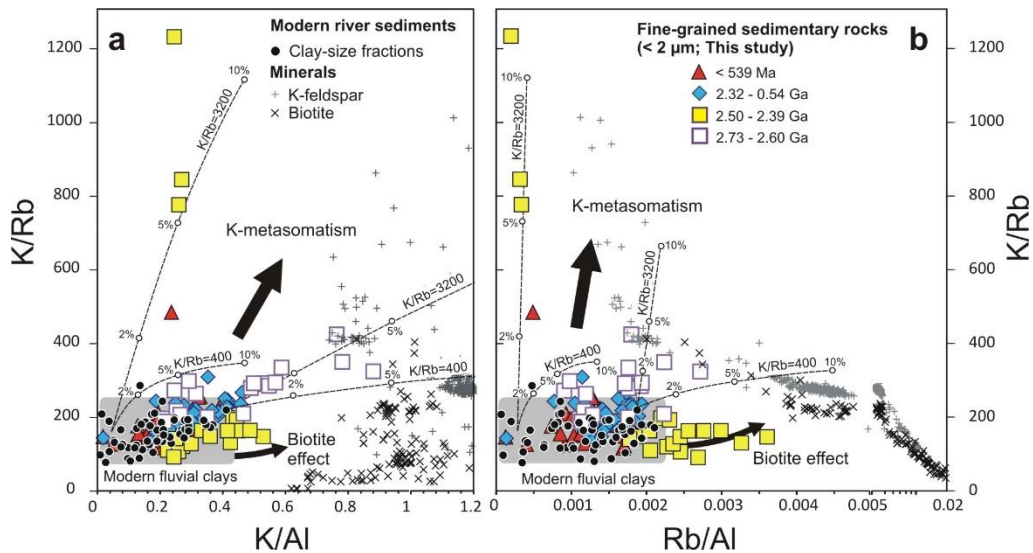
Figure 4. Relationship among K/Rb, K/Al, and Rb/Al in clay-size fraction of fine-grained sedimentary rocks. **a,** K/Rb versus K/Al. **b,** K/Rb versus Rb/Al. Most investigated shales plot within the field defined by modern river clays, characterized by K/Rb <240, K/Al <0.42, and Rb/Al <0.0022 (Bayon et al., 2021). Samples with K/Rb >240 are considered to be influenced by post-depositional metasomatic alteration, and hence were excluded from discussion. Theoretical curves illustrating the effect of metasomatic alteration on detrital clays are shown for comparison (with % indicating the percentage of K added after deposition), using fluid composition of K/Rb = 3200 for seawater and K/Rb = 400 for Rb-enriched fluid. Note that 2.50-2.39 Ga samples with Rb/Al >0.0022 and K/Rb <200 are linked to incongruent dissolution of biotite (see black arrow indicating 'biotite effect'). Also shown for comparison are data for K-feldspar and biotite from the Georoc database (http://georoc.mpch-mainz.gwdg.de/georoc/). Data for clay-size fraction of studied shales and modern fluvial sediments are listed in Tables S2 and S4, respectively.
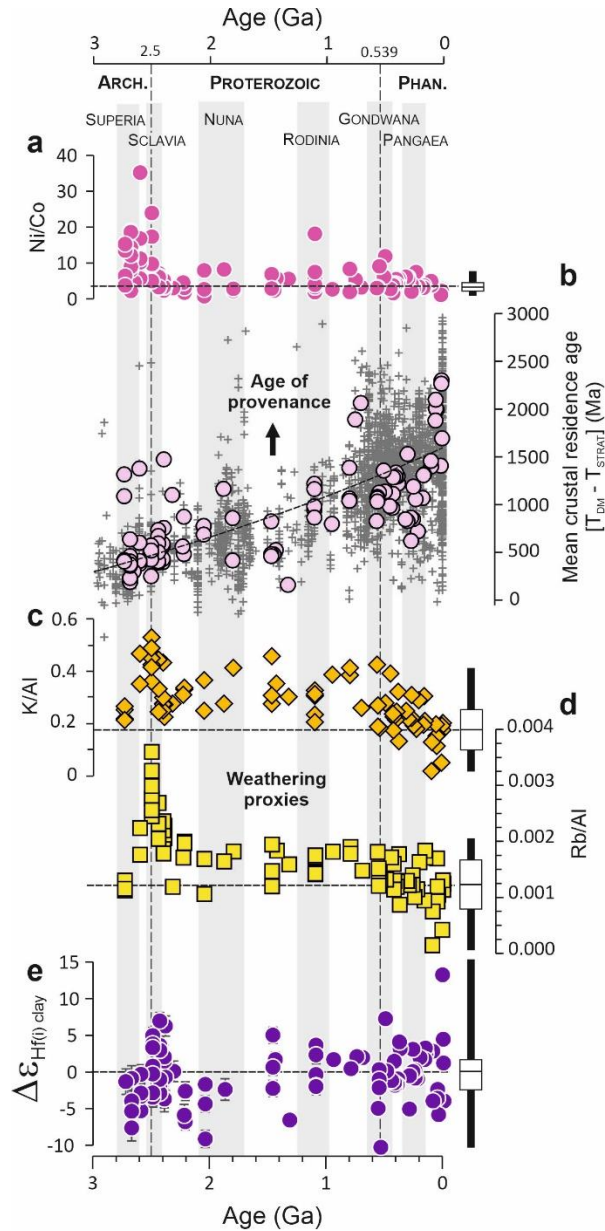
Figure 5. Evolution of Hf isotope composition of clay-size fraction and other sedimentary proxies for intensity of chemical weathering and provenance age and composition over the last ~2.7 Ga. **a,** Ni/Co ratios in clay-size fraction, as a provenance tracer for ultramafic vs. mafic and felsic crustal materials. **b,** Mean crustal residence time vs. depositional age of studied samples. Mean crustal residence time corresponds to the difference between Nd model age (T_{DM}) and depositional age (T_{DEP}), which provides an estimate for the age of eroded crustal materials at the time of sediment deposition. Pink circles correspond to data for clay-size

fraction (this study) and grey crosses refer to literature data for siliciclastic rocks (Garçon, 2021, and references therein), with a dashed line representing the best-fit polynomial regression (R^2=0.45). **c,** K/Al ratio of clay-size fraction is shown as a proxy for feldspar chemical weathering intensity. **d,** Rb/Al ratio of clay-size fraction is used here as a tracer for weathering intensity of K-feldspar and micas (e.g., biotite). **e,** $\Delta\varepsilon_{Hf\,(i)CLAY}$ reflects the relative proportion of secondary clays to detrital, unweathered minerals in clay-size fractions. Positive $\Delta\varepsilon_{Hf\,(i)CLAY}$ values reflect preferential dissolution of Lu-rich minerals, such as apatite. Vertical grey bars refer to periods of supercontinent assembly characterized by enhanced crustal growth (Cawood and Hawkesworth, 2015), which are associated with erosion of relatively juvenile rocks characterized by radiogenic Nd-Hf compositions, hence resulting in low mean crustal residence time. Horizontal dashed lines correspond to mean average values for clay-size fraction of modern fluvial sediments (Table S4). The range of Ni/Co, K/Al, Rb/Al, and $\Delta\varepsilon_{Hf\,CLAY}$ for modern fluvial clays is shown for comparison (black box-and-whisker plots).
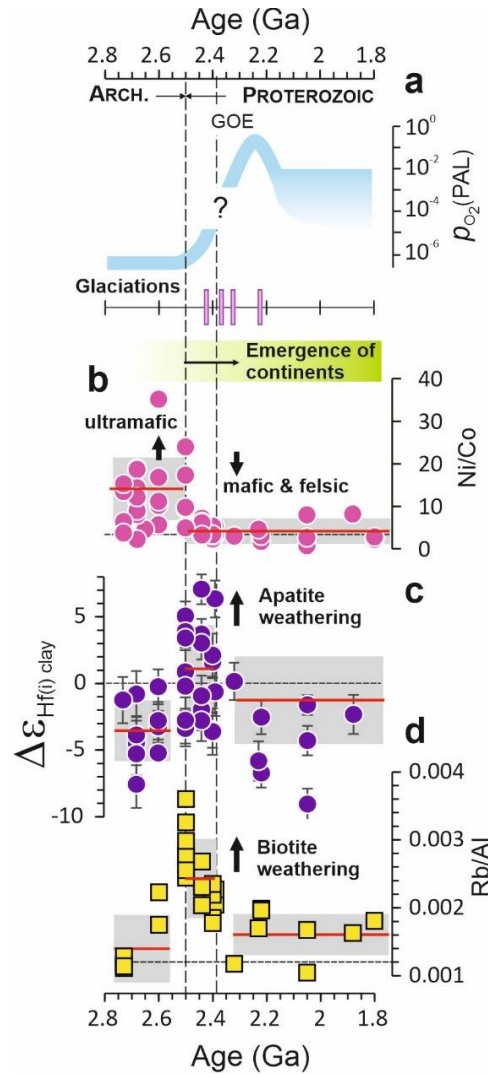
Figure 6. Trends in provenance and weathering proxies for clay-size fraction of the ~2.7 to 1.8 Ga shales in the context of Earth's oxygenation. **a,** Evolution of atmospheric oxygen, expressed as pO$_2$ relative to the present atmospheric level, PAL (Lyons et al., 2011; Catling and Zahnle, 2020). GOE refers to the Great Oxidation Event between ~2.45 and 2.1 Ga. The timeline of Paleoproterozoic glaciations and emergence of large continental landmasses is also shown. **b,** Ni/Co ratios in clay-size fraction, as a provenance tracer for ultramafic vs. mafic and felsic crustal materials. **c,** $\Delta\varepsilon_{Hf\,(i)CLAY}$, and **d,** Rb/Al, as chemical weathering proxies of clay-size fraction of sedimentary rocks. The rise of pO$_2$ from the Archean low level (<0.001% PAL; Pavlov and Kasting, 2002) is associated with a shift in $\Delta\varepsilon_{Hf\,(i)CLAY}$ and Rb/Al towards higher values, indicative of increased chemical weathering of apatite (or other easily altered Lu-rich

minerals) from subaerial, juvenile, mafic volcanic rocks and incongruent dissolution of biotite from the upper continental crust. Horizontal red lines (and associated grey boxes) correspond to the average values (± 1 SD) for the periods of ~2.73-2.50 Ga, ~2.50-2.39 Ga, and ~2.3-0.7 Ga. Horizontal dashed lines correspond to mean average values for clay-size fraction of modern fluvial sediments (Table S4).
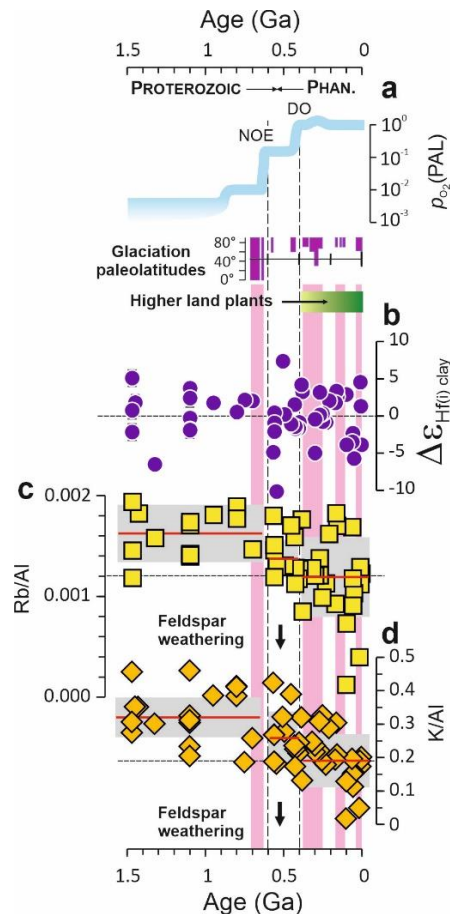
Figure 7. Trends in weathering proxies for clay-size fraction of shales in the context of Earth's oxygenation over the last 1.5 Ga. **a,** Evolution of atmospheric oxygen (pO$_2$ relative to PAL; Catling and Zahnle, 2020). NOE and DO refer to the Neoproterozoic and Devonian oxygenation events, respectively. The timeline for major Neoproterozoic and Phanerozoic glaciations (and their latitudinal extent; Mills et al., 2017) and appearance of the first vascular plants on land are shown for comparison. Vertical pink bars indicate relatively cold climate periods. $\Delta\varepsilon_{Hf\ (i)CLAY}$ (**b**), Rb/Al (**c**), and K/Al (**d**) are chemical weathering proxies for clay-size fraction of sedimentary rocks. The stepwise rise in pO$_2$ level in the late Neoproterozoic led to enhanced weathering of resistant silicate minerals such as feldspars from ~0.6 Ga. Horizontal red lines (and associated grey boxes) correspond to the average values (± 1 SD) for the ~2.3-0.7, 0.6-0.4, and <0.4 Ga periods. Horizontal dashed lines correspond to the mean average values for modern fluvial clays (Table S4).

References

Abbott, A.N., Löhr, S., & Trethewy, M., 2019. Are clay minerals the primary control on the oceanic rare earth element budget?. Front. Mar. Sci., 504.

Allègre, C.J., Rousseau, D., 1984. The growth of the continent through geological time studied by Nd isotope analysis of shales. Earth Planet. Sci. Lett. 67, 19-34.

Anbar, A.D., Duan, Y., Lyons, T.W., Arnold, G.L., Kendall, B., Creaser, R.A., Kaufman, A.J., Gordon, G.W., Scott, C., Garvin, J., Buick, R., 2007. A whiff of oxygen before the great oxidation event?. Science 317, 1903-1906.

Basu, A., 1981. Weathering before the advent of land plants: Evidence from unaltered detrital K-feldspars in Cambrian-Ordovician arenites. Geology 9, 132-133.

Bayon, G., Vigier, N., Burton, K.W., Jean Carignan, A.B., Etoubleau, J., Chu, N.C., 2006. The control of weathering processes on riverine and seawater hafnium isotope ratios. Geology 34, 433-436.

Bayon, G., Skonieczny, C., Delvigne, C., Toucanne, S., Bermell, S., Ponzevera, E., André, L., 2016. Environmental Hf–Nd isotopic decoupling in World river clays. Earth Planet. Sci. Lett. 438, 25-36.

Bayon, G., Freslon, N., Germain, Y., Bindeman, I.N., Trinquier, A., Barrat, J.A., 2021. A global survey of radiogenic strontium isotopes in river sediments. Chem. Geol. 559, 119958.

Bekker, A. ,Holland, H.D., 2012. Oxygen overshoot and recovery during the early Paleoproterozoic. Earth Planet. Sci. Lett. 317, 295-304.

Bindeman, I.N., Zakharov, D.O., Palandri, J., Greber, N.D., Dauphas, N., Retallack, G.J., Hofmann, A., Lackey, J.S., Bekker, A., 2018. Rapid emergence of subaerial landmasses and onset of a modern hydrologic cycle 2.5 billion years ago. Nature 557, 545-548.

Bleeker, W., 2003. The late Archean record: a puzzle in ca. 35 pieces. Lithos 71, 99-134.

Catling, D.C., Zahnle, K.J., 2020. The Archean atmosphere. Sci. Adv. 6, eaax1420.

Cawood, P.A., Hawkesworth, C.J., 2015. Temporal relations between mineral deposits and
global tectonic cycles. Geol. Soc. Lond. Sp. Pub. 393, 9-2.

Condie, K.C., 1993. Chemical composition and evolution of the upper continental crust:
contrasting results from surface samples and shales. Chem. Geol. 104, 1-37.

Condie, K.C., 2004. Supercontinents and superplume events: distinguishing signals in the
geologic record. Phys. Earth Planet. Int. 146, 319-332.

Corentin, P., Pucéat, E., Pellenard, P., Freslon, N., Guiraud, M., Blondet, J., Adatte, T.,
Bayon, G., 2022. Hafnium-neodymium isotope evidence for enhanced weathering and
uplift-climate interactions during the Late Cretaceous. Chem. Geol., 120724.

Cox, R., Lowe, D.R., Cullers, R.L., 1995. The influence of sediment recycling and basement
composition on evolution of mudrock chemistry in the southwestern United States.
Geochim. Cosmochim. Acta 59, 2919-2940.

Dahl, T.W., Hammarlund, E.U., Anbar, A.D., Bond, D.P., Gill, B.C., Gordon, G.W., Knoll,
A.H., Nielsen, A.T., Schovsbo, N.H., Canfield, D.E., 2010. Devonian rise in
atmospheric oxygen correlated to the radiations of terrestrial plants and large predatory
fish. Proc. Nat. Acad. Sci. 107, 17911-17915.

Dausmann, V., Gutjahr, M., Frank, M., Kouzmanov, K., Schaltegger, U., 2019. Experimental
evidence for mineral-controlled release of radiogenic Nd, Hf and Pb isotopes from
granitic rocks during progressive chemical weathering. Chem. Geol. 507, 64-84.

Dere, A.L., White, T.S., April, R.H., Reynolds, B., Miller, T.E., Knapp, E.P., McKay, L.D.,
Brantley, S.L., 2013. Climate dependence of feldspar weathering in shale soils along a
latitudinal gradient. Geochim. Cosmochim. Acta 122, 101-126.

Dessert, C., Dupré, B., Gaillardet, J., François, L.M., Allegre, C.J., 2003. Basalt weathering
laws and the impact of basalt weathering on the global carbon cycle. Chem. Geol. 202,
257-273.

Erel, Y., Blum, J.D., Roueff, E., Ganor, J., 2004. Lead and strontium isotopes as monitors of
experimental granitoid mineral dissolution. Geochim. Cosmochim. Acta 68, 4649-4663.

Ernst, R.E., Bond, D.P., Zhang, S.H., Buchan, K.L., Grasby, S.E., Youbi, N., El Bilali, H.,
Bekker, A., Doucet, L.S., 2021. Large Igneous Province Record Through Time and
Implications for Secular Environmental Changes and Geological Time-Scale
Boundaries. Large Igneous Provinces: A Driver of Global Environmental and Biotic
Changes, pp.1-26.

Fedo, C.M., Nesbitt, H.W., Young, G.M., 1995. Unraveling the effects of potassium
metasomatism in sedimentary rocks and paleosols, with implications for
paleoweathering conditions and provenance. Geology 23, 921-924.

Gaillardet, J., Dupré, B., Allègre, C.J., 1999. Geochemistry of large river suspended
sediments: silicate weathering or recycling tracer?. Geochim. Cosmochim. Acta 63,
4037-4051.

Garçon, M., Chauvel, C., France-Lanord, C., Huyghe, P., Lavé, J., 2013. Continental
sedimentary processes decouple Nd and Hf isotopes. Geochim. Cosmochim. Acta 121,
177-195.

Garçon, M., 2021. Episodic growth of felsic continents in the past 3.7 Ga. Sci. Adv. 7,
eabj1807.

Goyne, K.W., Brantley, S.L,. Chorover, J., 2006. Effects of organic acids and dissolved
oxygen on apatite and chalcopyrite dissolution: Implications for using elements as
organomarkers and oxymarkers. Chem. Geol. 234, 28-45.

Greber, N.D., Dauphas, N., Bekker, A., Ptáček, M.P., Bindeman, I.N., Hofmann, A., 2017. Titanium isotopic evidence for felsic crust and plate tectonics 3.5 billion years ago. Science 357, 1271-1274.

Guidry, M.W., Mackenzie, F.T., 2000. Apatite weathering and the Phanerozoic phosphorus cycle. Geology 28, 631-634.

Hoffmann, J.E., Münker, C., Polat, A., König, S., Mezger, K., Rosing, M.T., 2010. Highly depleted Hadean mantle reservoirs in the sources of early Archean arc-like rocks, Isua supracrustal belt, southern West Greenland. Geochim. Cosmochim. Acta 74, 7236-7260.

Isson, T.T., Planavsky, N.J., 2018. Reverse weathering as a long-term stabilizer of marine pH and planetary climate. Nature 560, 471-475.

Kennedy, M., Droser, M., Mayer, L.M., Pevear, D., Mrofka, D., 2006. Late Precambrian oxygenation; inception of the clay mineral factory. Science 311, 1446-1449.

Konhauser, K.O., Lalonde, S.V., Planavsky, N.J., Pecoits, E., Lyons, T.W., Mojzsis, S.J., Rouxel, O.J., Barley, M.E., Rosiere, C., Fralick, P.W., Kump, L.R., 2011. Aerobic bacterial pyrite oxidation and acid rock drainage during the Great Oxidation Event. Nature 478, 369-373.

Kump, L.R., Barley, M.E., 2007. Increased subaerial volcanism and the rise of atmospheric oxygen 2.5 billion years ago. Nature 448, 1033-1036.

Lenton, T.M., Crouch, M., Johnson, M., Pires, N., Dolan, L., 2012. First plants cooled the Ordovician. Nat. Geosci. 5, 86-89.

Lenton, T.M., Dahl, T.W., Daines, S.J., Mills, B.J., Ozaki, K., Saltzman, M.R., Porada, P., 2016. Earliest land plants created modern levels of atmospheric oxygen. Proc. Nat. Acad. Sci. 113, 9704-9709.

Lyons, T.W., Reinhard, C.T., Planavsky, N.J., 2014. The rise of oxygen in Earth's early ocean and atmosphere. Nature 506, 307-315.

Macdonald, F.A., Swanson-Hysell, N.L., Park, Y., Lisiecki, L., Jagoutz, O., 2019. Arc-continent collisions in the tropics set Earth's climate state. Science 364, 181-184.

McLennan, S.M., Simonetti, A., Goldstein, S.L., 2000. Nd and Pb isotopic evidence for provenance and post-depositional alteration of the Paleoproterozoic Huronian Supergroup, Canada. Precambrian Res. 102, 263-278.

Merdith, A.S., Williams, S.E., Collins, A.S., Tetley, M.G., Mulder, J.A., Blades, M.L., Young, A., Armistead, S.E., Cannon, J., Zahirovic, S., Müller, R.D., 2021. Extending full-plate tectonic models into deep time: Linking the Neoproterozoic and the Phanerozoic. Earth Sci. Rev. 214, 103477.

Michalopoulos, P., Aller, R.C., 1995. Rapid clay mineral formation in Amazon delta sediments: reverse weathering and oceanic elemental cycles. Science 270, 614-617.

Murakami, T., Ito, J.I., Utsunomiya, S., Kasama, T., Kozai, N., Ohnuki, T., 2004. Anoxic dissolution processes of biotite: implications for Fe behavior during Archean weathering. Earth Planet. Sci. Lett. 224, 117-129.

Neaman, A., Chorover, J., Brantley, S.L., 2005. Element mobility patterns record organic ligands in soils on early Earth. Geology 33, 117-120.

Nesbitt, H.W., Markovics, G., 1980. Chemical processes affecting alkalis and alkaline earths during continental weathering. Geochim. Cosmochim. Acta 44, 1659-1666.

Ohr, M., Halliday, A.N., Peacor, D.R., 1994. Mobility and fractionation of rare earth elements in argillaceous sediments: implications for dating diagenesis and low-grade metamorphism. Geochim. Cosmochim. Acta 58, 289-312.

Ostrander, C.M., Johnson, A.C., Anbar, A.D., 2021. Earth's First Redox Revolution. Annu. Rev. Earth Planet. Sci. 49, 337-366.

Patchett, P.J., White, W.M., Feldmann, H., Kielinczuk, S., Hofmann, A.W., 1984. Hafnium/rare earth element fractionation in the sedimentary system and crustal recycling into the Earth's mantle. Earth Planet. Sci. Lett. 69, 365-378.

Pavlov, A.A., Kasting, J.F., 2002. Mass-independent fractionation of sulfur isotopes in Archean sediments: strong evidence for an anoxic Archean atmosphere. Astrobiology 2, 27-41.

Planavsky, N.J., Rouxel, O.J., Bekker, A., Lalonde, S.V., Konhauser, K.O., Reinhard, C.T., Lyons, T.W., 2010. The evolution of the marine phosphate reservoir. Nature 467, 1088-1090.

Rafiei, M., Kennedy, M., 2019. Weathering in a world without terrestrial life recorded in the Mesoproterozoic Velkerri Formation. Nat. Commun. 10, 1-9.

Rafiei, M., Löhr, S., Baldermann, A., Webster, R., Kong, C., 2020. Quantitative petrographic differentiation of detrital vs diagenetic clay minerals in marine sedimentary sequences: Implications for the rise of biotic soils. Precambrian Res. 350, 105948.

Rasmussen, B., Fletcher, I.R., Sheppard, S., 2005. Isotopic dating of the migration of a low-grade metamorphic front during orogenesis. Geology 33, 773-776.

Raymo, M.E., Ruddiman, W.F., 1992. Tectonic forcing of late Cenozoic climate. Nature 359, 117-122.

Reinhard, C.T., Planavsky, N.J., Gill, B.C., Ozaki, K., Robbins, L.J., Lyons, T.W., Fischer, W.W., Wang, C., Cole, D.B., Konhauser, K.O., 2017. Evolution of the global phosphorus cycle. Nature 541, 386-389.

Retallack, G.J., Chen, Z.-Q., Huan, Y, Feng, H. Y., 2021. Mesoproterozoic alluvial paleosols of the Ruyang group in Henan, China. Precambrian Res. 364, 106361.

Schott, J., Berner, R.A., 1985. Dissolution mechanisms of pyroxenes and olivines during weathering, in: Drever, J.I. (Ed.), The chemistry of weathering. Springer, pp. 35-53.

Shields, G., Veizer, J., 2002. Precambrian marine carbonate isotope database: Version 1.1. Geochem. Geophys. Geosyst. 3. https://doi.org/10.1029/2001GC000266

Slotznick, S.P., Johnson, J.E., Rasmussen, B., Raub, T.D., Webb, S.M., Zi, J.W., Kirschvink, J.L., Fischer, W.W., 2022. Reexamination of 2.5-Ga "whiff" of oxygen interval points to anoxic ocean before GOE. Sci. Adv. 8, eabj7190.

Stille, P., Clauer, N., 1994. The process of glauconitization: chemical and isotopic evidence. Contrib. Min. Petrol. 117, 253-262.

van de Kamp, P.C., 2016. Potassium distribution and metasomatism in pelites and schists: how and when, relation to postdepositional events. J. Sedim. Res. 86, 683-711.

Vervoort, J.D., Patchett, P.J., Blichert-Toft, J., Albarède, F., 1999. Relationships between Lu–Hf and Sm–Nd isotopic systems in the global sedimentary system. Earth Planet. Sci. Lett. 168, 79-99.

Vervoort, J.D., Plank, T., Prytulak, J., 2011. The Hf–Nd isotopic composition of marine sediments. Geochim. Cosmochim. Acta 75, 5903-5926.